Proceedings of the 2nd ITB Graduate School Conference

Strengthening Multidisciplinary Research to Enhance its Impact on Society
July 21, 2022

Numerical Simulation of Two-dimensional Vortex-Induced Vibration of Circular Cylinder Using Least Square Moving Particle Semi-Implicit Method – Vortex Particle Method (LSMPS-VPM)

Al-Faisal Firdaus* & Lavi Rizki Zuhal

Faculty of mechanical and Aerospace Engineering, Bandung Institute of Technology *Email: icalfirdaus12@gmail.com

Abstract. Interaction between fluid and structure is a complex problem that is often encountered in various engineering fields. One of the fluid-structure interaction (FSI) phenomena is vortex-induced vibration (VIV). In this research, a particle-based numerical method known as the Least square moving particle semiimplicit - Vortex particle method (LSMPS-VPM) was improved to be able to simulate the VIV of a solid rigid object. LSMPS-VPM utilized multi-resolution particles, LSMPS spatial operator, and the Brinkmann penalization method for directly solving Navier-Stokes equations in vorticity form. The LSMPS-VPM was improved by adding a VIV solver which employed the 4th order Runge-Kutta method to solve the one-degree-of-freedom vibration equation. The numerical method was tested with two benchmark problems: the flow past a static twodimensional circular cylinder and the VIV of a two-dimensional circular cylinder. The results of the static simulation show that the present method is already capable of producing results that agree with past simulations. On the other hand, from the results of the VIV simulation, the present method is capable of predicting the motion of the solid body immersed in the fluid, however, some parameters still show inaccurate results compared with the references.

Keywords: particle-based simulation; least square moving particle semi-implicit; vortex-induced vibration.

1 Introduction

Vortex-induced vibration (VIV) of a structure is one of the practical interests of many engineering fields. VIV is classified as a complex fluid-structure interaction (FSI) case where the vibration is induced by the generation of vortex shedding from the structure. VIV phenomenon can cause damage and sometimes can lead to structural failures. Hence, a comprehensive understanding of VIV is very important in designing and improving a structure's strength.

VIV phenomenon has been studied intensively in the past two decades. Comprehensive reviews of the fundamentals of VIV can be found in many

ISSN: 2963-718X

publications such as Sarpkaya [1] and Williamson [2]. Recently, various numerical simulations have been widely used to contribute to studying the nature of VIV and FSI in general. Most of the numerical simulations that are used in studying the VIV phenomenon are based on the grid-based method. Shen et al. [3] utilized the SIMPLEC algorithm coupled with immersed boundary method to simulate case studies for a static and a one-degree-of-freedom (1DOF) circular cylinder immersed in a fluid. Zhao et al. [4] investigated the VIV of a circular cylinder in oscillatory flow using Petrov-Galerkin finite element method. Pan et al. [5] utilized Reynolds averaged Navier-Stokes simulation code to simulate the VIV of a circular cylinder at a low mass-damping configuration. Pastrana et al. [6] simulated a VIV of a low-mass ratio two-degree-of-freedom circular cylinder at subcritical Reynolds numbers using Large-eddy simulation.

Although the use of the grid-based method is more prevalent in VIV simulation, the method may encounter difficulties when dealing with problems involving large deformation or complex body shapes [7]. To overcome the difficulties, a particle-based method can be utilized. The particle-based method provides advantages for complex domain simulation or high deformation simulation due to the usage of freely moving particles inside the simulation domain.

In this research, a particle-based simulation program for a simulation of VIV will be developed. The Least square moving particle semi-implicit – Vortex particle method (LSMPS-VPM) developed by Pristiansyah [8] will be used as the base program for this research. The LSMPS-VPM utilizes Least square moving particle semi-implicit (LSMPS) spatial operators [9] and the fast multipole method (FMM) [10], allowing multi-resolution particles and faster computational time compared with the classical VPM [11]. The present numerical method will be validated using benchmark test cases that have been done in the past research: simulation of a flow past static and 1DOF circular cylinder at Reynolds number 100. The remainder of this report is organized as follows: the present numerical method is explained in Section 2, the simulation details are presented in Section 3, and the results are discussed in Section 4, followed by the conclusions in Section 5.

2 Numerical Methods

2.1 Vortex Particle Method

The continuity and momentum equations for a viscous incompressible fluid are expressed as

$$\nabla \cdot \boldsymbol{u} = 0 \tag{1}$$

$$\frac{\partial u}{\partial t} + (\mathbf{u} \cdot \nabla)\mathbf{u} = -\frac{1}{\rho} \nabla p + \nu \nabla^2 \mathbf{u}$$
 (2)

where p is the pressure, u is the velocity vector, v is the kinematic viscosity, and ρ is the fluid density. The vorticity form of Eq. (2), can be obtained by taking the curl operation on both sides of Eq. (2)

$$\frac{\partial \boldsymbol{\omega}}{\partial t} + (\boldsymbol{u} \cdot \nabla) \boldsymbol{\omega} = (\boldsymbol{\omega} \cdot \nabla) \boldsymbol{u} + \nu \nabla^2 \boldsymbol{\omega}$$
 (3)

where ω is the vorticity defined by the curl of the velocity

$$\boldsymbol{\omega} = \nabla \times \boldsymbol{u} \tag{4}$$

For two-dimensional simulation in a Cartesian coordinate plane, $\mathbf{u} = (u, v)$ and $\mathbf{\omega} = \omega_z \hat{k}$, the stretching term $(\mathbf{\omega} \cdot \nabla)\mathbf{u}$ in the right-hand side of Eq. (3) disappears. Therefore, the momentum equation can be rewritten into

$$\frac{\partial \boldsymbol{\omega}}{\partial t} + (\boldsymbol{u} \cdot \nabla) \boldsymbol{\omega} = \frac{D \boldsymbol{\omega}}{Dt} = \nu \nabla^2 \boldsymbol{\omega}$$
 (5)

where $\frac{D}{Dt}$ is the material derivative. In the Vortex particle method (VPM), particles carrying vorticity are used to discretize the fluid. The discretized particle can be written mathematically as follows:

$$\omega_i = \Gamma_i V_i \tag{6}$$

where Γ_i and V_i are the vorticity strength and the volume of the corresponding ith particle. To obtain the solution of Eq. (5), the viscous splitting algorithm [12] is utilized. The algorithm includes two steps: convection and diffusion steps. These steps are described mathematically as follows:

$$\frac{dx}{dt} = \boldsymbol{u}(\boldsymbol{x}, t) \tag{7}$$

$$\frac{d\omega}{dt} = \nu \nabla^2 \omega(\mathbf{x}, t) \tag{8}$$

where x is the particle position vector. The Forward time-stepping scheme is used as the time integration method for Eq. (7) and (8). The stability condition of the scheme will be following the condition used by Ploumhans and Winckelmans [13].

To solve Eq. (7) and (8), the value of velocity field \boldsymbol{u} must be known. The velocity field is obtained by solving the Poisson equation constructed from the continuity equation (Eq. (1)) and the vorticity definition (Eq. (4))

$$\nabla^2 \mathbf{u} = -\nabla \times \boldsymbol{\omega} \tag{9}$$

One of the approaches to solve Eq. (9) and obtained the velocity field is to utilize the Green's function method [14]. Using this approach, the velocity field can be divided into several contributions, namely, irrotational velocity u_{∞} , and rotational velocity u_{∞} .

$$\boldsymbol{u} = \boldsymbol{u}_{\infty} + \boldsymbol{u}_{\omega} \tag{10}$$

For two-dimensional flow simulation, u_{∞} is the summation of the uniform flow velocity U_{∞} and the solid body velocity u_s . On the other hand, u_{ω} can be calculated as the sum of vorticities of the vortex elements,

$$\mathbf{u}_{\omega} = -\frac{1}{2\pi} \sum_{i=0}^{N} \frac{(x - x_i)}{|x - x_i|^2} \times \Gamma_i e_z \tag{11}$$

where e_z is the unit vector in the z-direction of a Cartesian coordinate system. The most common way to effectively compute Eq. (11) is by using the Fast multipole method (FMM) introduced by Greengard and Rokhlin in [15]. The detail of the FMM algorithm can be referred to in more detail in [15] and [10]. In this research, a well-developed FMM program is utilized to drastically reduce the computational time.

2.2 Least Squares Moving Particle Semi-Implicit Spatial Operators

Least squares moving particle semi-implicit (LSMPS) method is a meshfree Langrangian approach for numerical analysis of incompressible flow that was developed by Tamai and Koshizuka [9]. The LSMPS method utilizes a weighted least square function to reduce errors that surface in the Moving particle semi-implicit method. There are two types of LSMPS spatial operators: LSMPS type A and type B. The main difference between type A and B is that LSMPS type B can be used to calculate operators at an arbitrary position.

In this research, the spatial derivatives calculation of LSMPS is used to replace the discretization-correction method (DC-PSE) that was commonly used in the VPM. By using LSMPS spatial operators, multi-resolution simulation can be done easily without the need for additional modeling [16]. The LSMPS spatial operators are also used in the remeshing process of the VPM, replacing the previous redistribution technique due to the LSMPS capability in interpolating field values. The formula of LSMPS spatial operators is as follows:

$$D_x f^h(x_i) = \boldsymbol{H}_i \boldsymbol{M}_i^{-1} \boldsymbol{b}_i$$
 (12)

where D_x is a differential operator, H_{rs} is matrix coefficient, M_i is a moment matrix, and b_i is a moment vector. For a two-dimensional case, the second-order formulation of LSMPS type A for a particle with diameter L_i are as follows:

$$D_{x} = \begin{bmatrix} \frac{\partial}{\partial x} & \frac{\partial}{\partial y} & \frac{\partial^{2}}{\partial^{2}x} & \frac{\partial}{\partial x\partial y} & \frac{\partial^{2}}{\partial^{2}y} \end{bmatrix}^{T}$$

$$(13)$$

$$H_{i} = \begin{bmatrix} L_{i}^{-1} & 0 & 0 & 0 & 0 \\ 0 & L_{i}^{-1} & 0 & 0 & 0 & 0 \\ 0 & 0 & 2L_{i}^{-2} & 0 & 0 & 0 \\ 0 & 0 & 0 & L_{i}^{-1} & 0 & 0 \\ 0 & 0 & 0 & 0 & 2L_{i}^{-2} \end{bmatrix}$$

$$(14)$$

$$M_{i} = \sum_{j \in \Lambda_{i}} \left[w(\|x_{j} - x_{i}\|) P\left(\frac{x_{j} - x_{i}}{r_{s}}\right) P^{T}\left(\frac{x_{j} - x_{i}}{r_{s}}\right) \right]$$

$$(15)$$

$$b_{i} = \sum_{j \in \Lambda_{i}} \left[w(\|x_{j} - x_{i}\|) P\left(\frac{x_{j} - x_{i}}{r_{s}}\right) \{f(x_{j}) - f(x_{i})\} \right]$$

$$(16)$$

$$P = [x \quad y \quad x^{2} \quad xy \quad y^{2}]^{T}$$

$$(17)$$

$$w(x, r_{eff}) = \begin{cases} 1 - \frac{\|x\|}{r_{eff}} & , 0 \leq \|x\| < r_{eff} \\ 0 & , \|x\| \geq r_{eff} \end{cases}$$

$$(18)$$

where r_{eff} is the mean support radius of the particle, r_s is the residual size of the particle, Λ_i is a set that contains the *ith* particle neighbors, and w is the weight function. The support radius of a particle can be calculated using Koshizuka and Tamai formulation suggested in [16].

$$r_{eff} = 3.5L_i$$
(19)

On the other hand, the LSMPS type B formulation can be found by changing Eq. (13), (14), (16), and (17) into the followings:

$$D_{x} = \begin{bmatrix} 1 & \frac{\partial}{\partial x} & \frac{\partial}{\partial y} & \frac{\partial^{2}}{\partial^{2} x} & \frac{\partial}{\partial x \partial y} & \frac{\partial^{2}}{\partial^{2} y} \end{bmatrix}^{T}$$
(20)

$$\mathbf{H}_{i} = \begin{bmatrix}
1 & 0 & 0 & 0 & 0 & 0 \\
0 & l_{i}^{-1} & 0 & 0 & 0 & 0 \\
0 & 0 & l_{i}^{-1} & 0 & 0 & 0 \\
0 & 0 & 0 & 2l_{i}^{-2} & 0 & 0 \\
0 & 0 & 0 & 0 & l_{i}^{-1} & 0 \\
0 & 0 & 0 & 0 & 2l_{i}^{-2}
\end{bmatrix}$$

$$\mathbf{b}_{i} = \sum_{j \in \Lambda_{i}} \left[w(\|x_{j} - x_{i}\|) \mathbf{P}\left(\frac{x_{j} - x_{i}}{r_{s}}\right) \{f(x_{j})\} \right]$$
(21)
$$\mathbf{P} = \begin{bmatrix} 1 & x & y & x^{2} & xy & y^{2} \end{bmatrix}^{T}$$
(23)

where l_i is the average particle diameter around the position x. In a multiresolution particle simulation, the mean support radius of ith particle r_i could be different with its neighboring particles r_j . This could make a one-way interaction between particles [16]. Therefore, the support domain radius of multi-resolution r_{ij} must be calculated by considering the size of neighboring particles surrounding the ith particle,

$$r_{ij} = \frac{r_i + r_j}{2} \tag{24}$$

With the implementation of LSMPS operators in the VPM, the numerical method will be further referenced as LSMPS-VPM.

2.3 Brinkmann Penalization Method

To provide the no-slip condition for the solid boundary in the simulation, LSMPS-VPM utilized the Brinkmann penalization method. The Brinkmann penalization method works by adding the penalization term into Eq. (5). This addition will penalize the difference between the solid and fluid to be as close as zero. The penalized momentum equation is as follows:

$$\frac{D\boldsymbol{\omega}}{Dt} = \nu \nabla^2 \boldsymbol{\omega} + \nabla \times (\lambda \chi (\boldsymbol{u}_S - \boldsymbol{u}))$$
(25)

where λ is the porosity of the solid, χ is the characteristics function that defines the region of penalization, and u_s is the solid body velocity. The values of χ is following a mask function introduced by Gazzola et al. [17],

$$\chi = \begin{cases} 0 & , r_n < r_e \\ \frac{1}{2} \left(1 + \frac{r_n}{r_e} + \frac{1}{\pi} \sin \left(\pi \frac{r_n}{r_e} \right) \right) & , -r_e \le r_n \le r_e \\ 1 & , r_n > r_e \end{cases}$$
(26)

where r_n is the normal particle distance to the nearest discrete solid body particles and r_e is the affected region distance. The r_e length used in the two-dimensional case is $r_e = 2\sqrt{2}\sigma$, where σ is the smallest particle size used in the simulation. In the LSMPS-VPM, the penalization process will be evaluated semi-implicitly using a split-step algorithm similar to the advection and diffusion process.

$$u_{pen} = \frac{u + \lambda \Delta t \chi u_s}{1 + \lambda \Delta t \chi}$$
(27)
$$\omega_{pen} = \nabla \times u_{pen}$$
(28)

where u_{pen} is the penalized velocity, ω_{pen} is the penalized vorticity, and Δt is the time increment. For the calculation of the curl of u_{pen} , LSMPS spatial operators will be used.

2.4 Aerodynamic Forces Calculation

The aerodynamics forces computed from the LSMPS-VPM utilized the penalization force due to the implemented Brinkmann penalization. The penalization force calculation method is expressed as

$$F = \rho \int_{\Omega} \lambda \chi(u - u_s) dS$$
(29)

where S is the area of the penalized domain. The lift (Cl) and drag (Cd) coefficients can be calculated by using the following equations,

$$Cl = \frac{F \cdot e_y}{\frac{1}{2}\rho U_\infty^2 D} \tag{30}$$

$$Cd = \frac{F \cdot e_x}{\frac{1}{2}\rho U_\infty^2 D} \tag{31}$$

where e_x and e_y are the unit vector in x and y direction of the Cartesian coordinate, and D is the reference length of the simulated object.

2.5 Vortex-Induced Vibration

The VIV simulation in this research will be considering the case of a structure that is attached to a spring and damper. The vibration of a structure in the traverse *y* direction in a Cartesian coordinate is governed by an ordinary differential equation as follows:

$$M\ddot{y} + C\dot{y} + Ky = F_y$$
(32)

where M is the mass of the structure, C is the damping constant, K is the spring constant, and F_y is the fluid force felt by the structure in the y-direction. The non-dimensional form of Eq. (31) is often used to perform numerical simulation because it provides a more valid definition for a certain occurring limitation.

$$M^*\ddot{y}^* + C^*\dot{y}^* + K^*y^* = F_y^* \tag{33}$$

where M^* is the non-dimensional mass, C^* is the non-dimensional damping constant, K^* is the non-dimensional spring constant, and y^* is the non-dimensional traverse y-direction. To solve Eq. (32), the 4^{th} order Runge-Kutta method will be utilized.

2.6 Numerical Procedure

To provide a clearer picture of the developed program calculation procedures, assuming the particle vorticity, the uniform flow velocity, and the solid body velocity values at time t are known, the values at $t + \Delta t$ can be computed as follows:

- Compute \mathbf{u}_{ω} using Eq. (11), then compute \mathbf{u} using Eq. (10).
- Penalize the obtained velocity field using Eq. (27).
- Correct the particle vorticity using Eq. (28) with the help of LSMPS spatial operators.
- Compute the forces exerted on the simulation object using Eq. (29)
- Do the advection step by integrating Eq. (7) and update the particle location
- Do the diffusion step by integrating Eq. (8) and update the vorticity value for each particle.
- Compute the effect of the force on the vibration of the object by solving Eq. (33) and update the solid object's location and velocity for the next time step.
- Remesh the particles back to their initial location and repeat the calculation for the next time step.

3 Problem Descriptions

The developed program is first evaluated using a simulation case of a flow around a static circular cylinder at Reynolds number ($Re = \frac{u_{\infty}D}{v}$) 100. The uniform flow velocity is set to be $U_{\infty} = 1$. The simulation domain is discretized by using a uniform multi-resolution particle arrangement, with the smallest particle size σ . The fluid density ρ will also be set to 1.

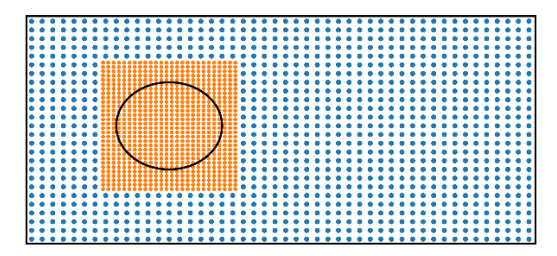


Figure 1 Example of multi-resolution particle distribution in LSMPS-VPM. Particle distribution is denser near the simulation object. The size of the smaller particles represented in orange is σ . On the other hand, the size of the bigger particles represented in blue is 4σ

Next, the VIV simulation of a circular cylinder will be conducted at the same *Re*. The particle size from the previous simulation which produced the most accurate results compared with the references will be used in the VIV simulation. The example of the particle distribution is shown in Figure 1.

In all of the simulation cases, a computational domain $[-7.5D, 30D] \times [-7.5D, 7,5D]$ will be used. The value of D refers to the diameter of the circular cylinder. The center of the cylinder will be placed at (0,0) for both simulation cases. The non-dimensional time is expressed as $T = \frac{U_{\infty}t}{D}$. To fulfill the stability condition, a non-dimensional time increment of $\Delta T = 0.007$ is selected for all the simulations. The simulations will be set to run for T = 120. The schematics of the simulation can be seen in Figure 2.

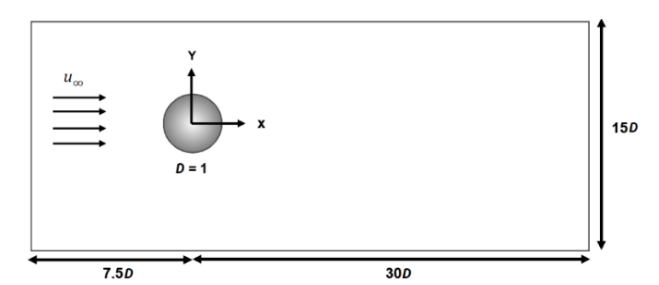


Figure 2 Schematics of the computational domain of flow past a circular cylinder.

4 Results and Discussions

4.1 Flow Around a Circular Cylinder

The present numerical simulation accuracy is investigated in this section using particle size convergence test. The test is carried out by using 3 different values of σ , mainly 0.05, 0.025, and 0.02. In the convergence test, the maximum lift coefficients Cl_{max} , mean lift coefficient $\bar{C}l$, mean drag coefficient $\bar{C}d$, and the Strouhal number St are the main parameters that will be analyze. The mean value of the variables is obtained at the fluctuation region of the simulation where the vortex shedding behind the cylinder is already in stable condition. The results of the simulations are shown in Table 1. From the results, it can be seen that the coefficients are getting closer to a certain number with the smaller value of σ . Therefore, the results of $\sigma = 0.02$ will be used as the LSMPS-VPM representative for comparison with other references.

Table 1 The results of particle size convergence test of LSMPS-VPM for flow around a static circular cylinder

No	σ	Cl_{max}	ĒΙ	Ēd	St
1	0.05	0.531	0.335	1.554	0.149
2	0.025	0.408	0.253	1.398	0.158
3	0.02	0.382	0.233	1.363	0.158

Table 2 shows the comparison of LSMPS-VPM with other references. From the comparison, it can be seen that the $\bar{C}d$ result of the present LSMPS-VPM is in good agreement with Shen et al. [3], and Nguyen et al. [18]. The St result of LSMPS-VPM is close to Nguyen et al. [18]. On the other hand, the Cl_{max} result of LSMPS-VPM shows a bigger result compared with the other references. However, the difference is not that high, with the highest being only 19.3% higher compared with Mimeau et al. [19]. With these results, it can be concluded

that the LSMPS-VPM can predict the Cd value well for a flow around a circular cylinder. LSMPS-VPM can also predict Cl and St values, but with a lower accuracy than the prediction of Cd.

Table 2 Maximum lift (Cl_{max}) , mean lift $(\bar{C}l)$, mean drag $(\bar{C}d)$ coefficients and Strouhal number (St) of a static circular cylinder immersed in the flow at Re = 100

Authors	Cl_{max}	ĒΙ	Ū́d	St
Present authors	0.382	0.233	1.363	0.158
Shiels et al. [20]	_	0.30	1.33	0.167
Shen et al. [3]	0.364	_	1.376	0.166
Mimeau et al. [19]	0.32	_	1.4	0.165
Yan et al. [21]	0.34	_	1.387	0.166
Nguyen et al. [18]	0.34	-	1.36	0.16

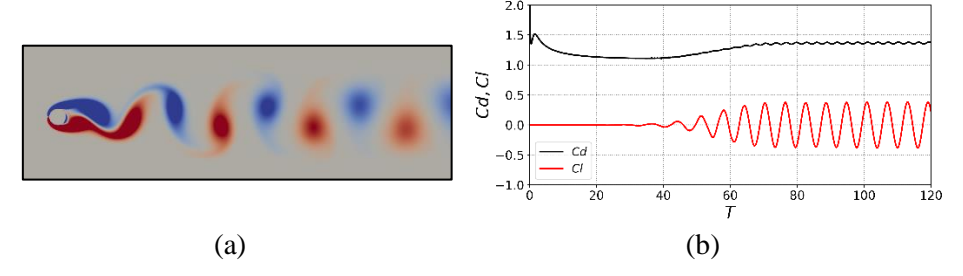


Figure 3 (a) Instantaneous vorticity distribution of the flow around a circular cylinder at Re = 100. Colorbar for the distribution is plotted in the range -1 to 1. (b) Time history of lift and drag coefficients (Cl and Cd).

Figure 3, shows the vorticity contours and the time history of Cl and Cd of the circular cylinder simulation. It is observed that the flow pattern behind the cylinder is resembling the Karman vortex street pattern. The fluctuations of the lift and drag coefficients are because there is a generation of vortex shedding behind the circular cylinder. From Figure 3(b), it can be seen that the vortex behind the cylinder is starting to shed at around T = 40.

4.2 Vortex-Induced Vibration of a Circular Cylinder.

In the VIV simulation, an elastically mounted rigid circular cylinder is constrained to move traversely to a uniform free-stream velocity. To observe the vibration of the cylinder due to the effect of the flow, an undamped simulation will be set. Similar parameters with the simulation of flow past a circular cylinder will be used in the VIV simulation. The smallest particle size inside the simulation domain will be set to be 0.02. For the mass and spring constant, the non-dimensional values from Shiels et al. [20] are selected. The vibration parameters used in the VIV simulation are listed in Table 3.

 Table 3
 Parameters for the VIV simulation

No	Parameters	Value
1	Non-dimensional mass M*	2.5
2	Non-dimensional spring constant K*	4.96
3	Non-dimensional damping constant C*	0.0

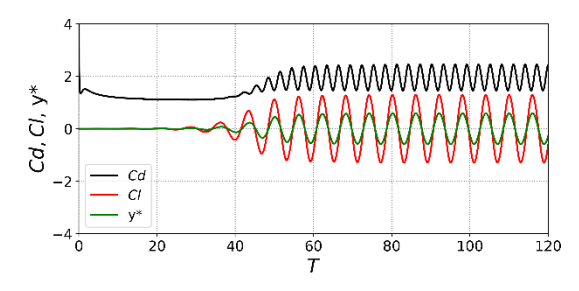


Figure 4 Time history of Cl, Cd, and y^* of two-dimensional VIV simulation of a circular cylinder at Re = 100.

At the start of the simulation, the cylinder was held steady until the flow passed the instability region at $T \ge 5$. After that, the vibration will be taken into account and the circular cylinder is allowed to move in y-direction. The Cl, Cd and y^* time history can be seen in Figure 4. The up and down motions of the cylinders are shown in Figure 5. These cylinder motions are followed by the generation of vortex sheds behind the wake of the cylinder. From Figures 4 and 5, it can be seen that the upward motion of the cylinder is followed by the increased value of Cl and vice versa. These phenomena are consistent throughout the simulation time. The vibration of the circular cylinder is already in stable condition at around T = 60.

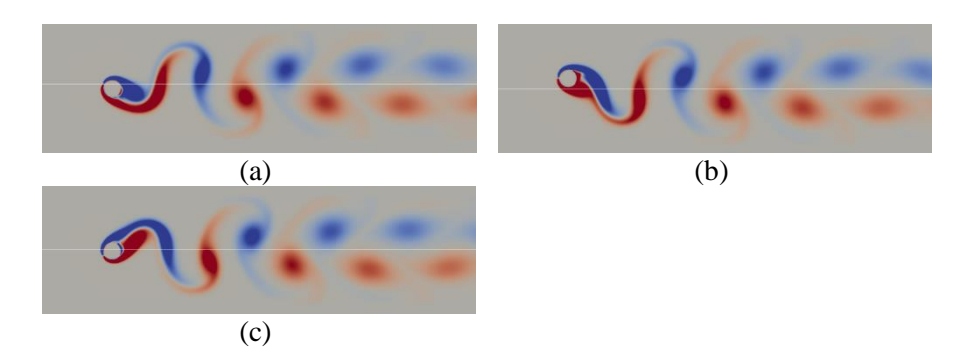


Figure 5 Vorticity distributions of the VIV simulation of a circular cylinder at Re = 100: (a) at T = 96.25, (b) at T = 98, and (c) at T = 99.75. The white line in the middle of each figure is the horizontal line where $y^* = 0$.

Table 4 shows the results of Cl_{max} , $\bar{C}d$, vibration amplitude A, and the motion frequency f of the circular cylinder for the current LSMPS-VPM and the selected references. The results of $\bar{C}d$ and A from LSMPS-VPM are slightly similar to both of the references. The results from Shiels et al. [20] show the largest difference in results for both $\bar{C}d$ and A of LSMPS-VPM with a difference of 10% and 1.38%, respectively. On the other hand, the LSMPS-VPM $\bar{C}l$ and f values are not in agreement with the references. The LSMPS-VPM result of Cl_{max} is way off compared with the references; with a difference of 68.83% higher compared with Shiels et al. [20] and 56.6% higher compared with Shen et al. [3]. Similarly, the LSMPS-VPM result of f is around 15.3% smaller compared with Shiels et al. [20]. From these results, it can be concluded that the present LSMPS-VPM is already capable of simulating the VIV phenomenon. However, several parameters still show results that are not in agreement with the references.

Table 4 Maximum lift (Cl_{max}), mean drag ($\bar{C}d$) coefficients, Amplitude of vibration (A), and vibration frequency (f) of the VIV simulation of a circular cylinder immersed in the fluid at Re = 100.

Authors	Cl_{max}	Ēd	Α	f
Present authors	1.3	1.998	0.588	0.166
Shiels et al	0.77	2.22	0.58	0.196
Shen et al.	0.83	2.15	0.57	0.19

5 Conclusions

The LSMPS-VPM has been successfully developed to be able to simulate a simple two-dimensional VIV simulation. The present numerical simulation has also been tested and validated with several references. The results of the static simulation are found to agree well with those available in the literature. The LSMPS-VPM is also accurately capable of simulating the vorticity generation behind the cylinder wake. Similarly, the VIV simulation results show a good representation of vorticity generation behind the circular cylinder. However, several results of the VIV simulation are not in good agreement with the selected references. This is because the movement of the cylinder adds more complexity to solving the Brinkmann penalization term. Thus, the penalization region did not penalize completely to as close as zero, making the force calculation slightly higher or lower compared to the references. Overall, the LSMPS-VPM is already capable of reproducing a representative natural phenomenon of vortex generation past a bluff body in both static and VIV simulation.

References

- [1] T. Sarpkaya, "A critical review of the intrinsic nature of vortex-induced vibrations," *Journal of Fluids and Structures*, vol. 19, no. 4, pp. 389-447, 2004.
- [2] C. Williamson and R. Govardhan, "A brief review of recent results in vortex-induced vibrations," *Journal of Wind Engineering and Industrial Aerodynamics*, vol. 96, no. 6-7, pp. 713-735, 2008.
- [3] L. Shen, E.-S. Chan and P. Lin, "Calculation of hydrodynamic forces acting on a submerged moving object," *Computer & Fluids*, vol. 38, pp. 691-702, 2009.
- [4] M. Zhao, L. Cheng and H. An, "Numerical investigation of vortex-induced vibration of a circular cylinder in transverse direction in oscillatory flow," *Ocean Engineering*, vol. 41, pp. 39-52, 2012.
- [5] Z. Y. Pan, W. Cui and Q. M. Miao, "Numerical simulation of vortex-induced vibration of a circular cylinder at low mass-damping using RANS code," *Journal of Fluids and Structures*, vol. 23, no. 1, pp. 23-37, 2007.
- [6] D. Pastrana, J. Cajas, O. Lehmkuhl, I. Rodriguez and G. Houzeaux, "Large-eddy simulations of the vortex-induced vibration of a low mass ratio two-degree-of-freedom circular cylinder at subcritical Reynolds numbers," *Computer & Fluids*, vol. 173, pp. 118-132, 2018.
- [7] W. A. Wall, A. Gerstenberger, P. Gamnitzer, C. Forster and E. Ramm, Large Deformation Fluid-Structure Interaction Advances in ALE Methods and New Fixed Grid Approaches, Berlin: Springer, 2006.
- [8] A. Pristiansyah, *Improvement of Vortex Particle Method using Multi-Resolution Least Square Moving Particle Semi-implicit (LSMPS) Method*, Bandung: Institut Teknologi Bandung, 2019.
- [9] T. Tamai and K. Seiichi, "Least squares moving particle semi-implicit method," *Computational Particle Mechanics*, vol. 1, no. 3, pp. 277-305, 2014.
- [10] T. Hrycak and V. Rokhlin, "An Improved Fast Multipole Algorithm for Potential Fields," *SIAM Journal on Scientific Computing*, vol. 19, no. 6, pp. 1804-1826, 1998.
- [11] G.-H. Cottet and P. D. Koumoutsakos, Vortex Methods: Theory and Practice, Cambridge University Press, 2000.
- [12] A. J. Chorin, "Vortex Sheet Approximation of Boundary Layers," *Journal of Computational Physics*, vol. 27, no. 3, pp. 428-442, 1978.

- [13] P. Ploumhans and G. Winckelmans, "Vortex Methods for High-Resolution Simulations of Viscous Flow Past Bluff Bodies of General Geometry," *Journal of Computational Physics*, vol. 165, no. 2, pp. 354-406, 2000.
- [14] C. Greengard, "The Core Spreading Vortex Method Approximates the Wrong Equation," *Journal of Computational Physics*, vol. 61, no. 2, pp. 345-348, 1985.
- [15] L. Greengard and V. Rokhlin, "A fast algorithm for particle simulations," *Journal of Computational Physics*, vol. 73, no. 2, pp. 325-348, 1987.
- [16] M. Tanaka, R. Cardoso and H. Bahai, "Multi-resolution MPS Method," *Journal of Computational Physics*, vol. 359, pp. 106-136, 2018.
- [17] M. Gazzola, P. Chatelain, W. M. van Rees and P. Koumoutsakos, "Simulations of single and multiple swimmers with non-divergence free deforming geometries," *Journal of Computational Physics*, vol. 230, no. 19, pp. 7093-7114, 2011.
- [18] V. L. Nguyen, T. Nguyen-Thoi and V. Duong, "Characteristics of the flow around four cylinders of various shapes," *Ocean Engineering*, vol. 238, 2021.
- [19] C. Mimeau, F. Gallizio, G.-H. Cottet and I. Mortazavi, "Vortex penalization method for bluff body flows," *Numerical Methods in Fluids*, vol. 79, no. 2, pp. 55-83, 2015.
- [20] D. Shiels, A. Leonard and A. Roshko, "Flow-induced Vibration of a Circular Cylinder at Limiting Structural Parameters," *Journal of Fluids and Structures*, vol. 15, no. 1, pp. 3-21, 2001.
- [21] H. Yan, G. Zhang, S. Wang, D. Hui and B. Zhou, "Simulation of Vortex Shedding Around Cylinders by Immersed Boundary-Lattice Boltzmann Flux Solver," *Applied Ocean Research*, vol. 114, 2021.
- [22] S. Koshizuka, K. Shibata, M. Kondo and T. Matsunaga, Moving Particle Semi-implicit Method: A Meshfree Particle Method for Fluid Dynamics, Academic Press, 2018.
- [23] L. G. R. and M. B. Liu, Smoothed Particle Hydrodynamics: A Meshfree Particle Method, World Scientific, 2003.
- [24] S. Birte, S. Reboux and I. Sbalzarini F., "Discretization correction of general integral PSE Operators for particle methods," *Journal of Computational Physics*, vol. 229, no. 11, pp. 4159-4182, 2010.
- [25] G. S. Winckelmans and A. Leonard, "Contributions to Vortex Particle Methods for the Computation of Three-Dimensional Incompressible Unsteady Flow," *Journal of Computational Physics*, vol. 109, no. 2, pp. 247-273, 1993.

- [26] L. J. Wicker and W. C. Skamarock, "Time-Splitting Methods for Elastic Models Using Forward Time Schemes," *Monthly Weather Review*, vol. 130, no. 8, pp. 2088-2097, 2002.
- [27] J. T. Rasmussen, G.-H. Cottet and J. H. Walther, "A multiresolution remeshed Vortex-In-Cell algorithm using patches," *Journal of Computational Physics*, vol. 230, no. 17, pp. 6472-6755, 2011.
- [28] E. Rossi, A. Colagrossi, D. Durante and G. Graziani, "Simulating 2D viscous flow around geometries with vertices through the Diffused Vortex Hydrodynamics method," *Computer Methods in Applied Mechanics and Engineering*, vol. 302, pp. 147-169, 2016.
- [29] V. D. Duong, L. R. Zuhal and H. Muhammad, "Fluid-structure coupling in time domain for dynamic stall using purely Lagrangian vortex method," *CEAS Aeronautical Journal*, vol. 12, pp. 381-399, 2021.